THE JOURNAL OF PHYSICAL CHEMISTRY B

Article

pubs.acs.org/JPCB

Ab Initio Study on an Excited-State Intramolecular Proton-Transfer Reaction in Ionic Liquid

Seigo Hayaki,[†] Yoshifumi Kimura,[‡] and Hirofumi Sato*,[†]

[†]Department of Molecular Engineering, Kyoto University, Kyoto Daigaku Katsura, Kyoto 615-8510, Japan

[‡]Department of Chemical Science and Technology, Hosei University, Koganei, 184-8584, Japan

Supporting Information

ABSTRACT: An excited-state intramolecular proton transfer (ESIPT) reaction of 4′-*N*,*N*-dimethylamino-3-hydroxyflavone in room temperature ionic liquid is theoretically investigated using RISM-SCF-SEDD, which is a hybrid method of molecular liquid theory and ab initio molecular orbital theory. The photo-excitation and proton-transfer processes are computed by considering the solvent fluctuation. The calculated absorption and emission energy are in good agreement with the experiments. The changes in the dipole moment indicate that the drastic solvation relaxation is accompanied by the excitation and an ESIPT process, which is consistent with the remarkable dynamic Stokes shift observed in the experiments. We calculated the nonequilibrium free-energy contour as a function of the proton coordinate and the solvation coordinate. We conclude that although immediately after the excitation the barrier height of the ESIPT process is relatively small, the barrier becomes larger as the solvation relaxation to the excited normal state proceeds. The solvation relaxation process is also investigated on the basis of microscopic solvation structure obtained by RISM calculations.

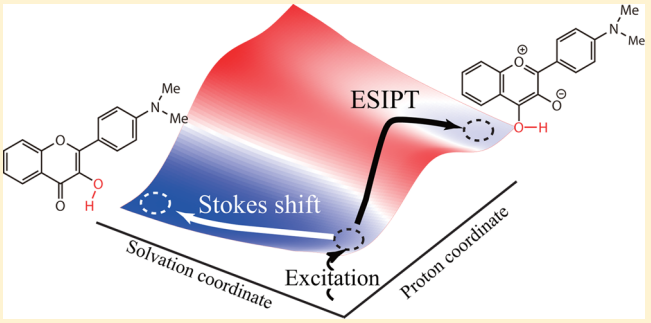

INTRODUCTION

Room-temperature ionic liquids (RTILs) have been extensively studied as a novel class of solvent.[1−4] The solvation dynamics of RTILs have attracted great attention from researchers, and its features have been clarified. In particular, one interesting feature is the wide distribution of solvation time scales.[5−13] Molecular dynamics simulations[14−16] suggest that the fastest component can be attributed to translational motions of the ions in the vicinity of the solute molecule.

The solvation dynamics[17,18] in an excited-state intramolecular proton transfer (ESIPT) reaction of 4′-*N*,*N*-diethylamino-3-hydroxyflavone (DEAHF) (Scheme 1) in RTILs has been studied with steady-state and time-resolved fluorescent spectroscopy.[19−21] Basically, the ESIPT kinetics in RTILs are similar to those in conventional solvent;[22−24] the proton-transfer rate shows noticeable dependence on the excitation wavelength.[20,21]

Scheme 1. Excited State Intramolecular Proton Transfer Reaction of DEAHF

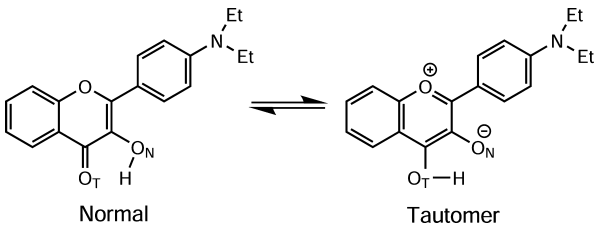

Several other works also report the excitation-wavelength dependence (red-edge-effect) in ionic liquid systems.[25−28] Although the molecular mechanism of this dependence was suggested,[21] the role of the solvation on the ESIPT reaction is still unclear.

In the field of theoretical chemistry, a hybrid method of quantum mechanics and molecular mechanics (QM/MM) is a straightforward approach to study the electronic structure of a molecule in solution phase. The QM/MM study of ionic liquid systems, however, is very limited so far because the strong Coulombic interactions among ions make it formidable to describe RTIL solvation properly, leading to large computational demands. Hence semiempirical methods, such as PM3, are mainly utilized to describe chemical reactions in RTILs,[29−33] except for one density functional theory (DFT) study.[34]

The reference interaction site model (RISM)[35,36] is an alternative way to tackle ionic liquid systems. Thanks to its analytical treatment of the correlation function, RISM is capable of taking into account the long-range Coulombic interaction and is free from statistical error. This theory has been expanded to multicomponent systems[37] and successfully applied to investigate solvation structures in the classical manner.[38,39] Not only static properties but also dynamic ones, such as the transport and relaxation processes of RTILs, have been explored using mode-

Received: December 3, 2012
Revised: March 27, 2013

ACS Publications © XXXX American Chemical Society

dx.doi.org/10.1021/jp311883f | J. Phys. Chem. B XXXX, XXX, XXX−XXX

coupling theory based on RISM.[40] RISM-SCF-SEDD[41−45] is a hybrid of RISM and ab initio molecular orbital theory, which enables us to pursue chemical phenomena in RTILs. KS-DFT/3D-RISM-KH[46] is a similar approach combining RISM and Kohn−Sham DFT. The effects of electronic polarization on solvation structures[47] and the mechanisms of chemical reactions in RTILs were clarified from first-principles.[48−50] It is also noted that RISM-SCF[41−43] was proved to be a powerful tool to obtain free-energy profiles along proton transfer reaction coordinates in solutions.[51−55]

We wish to report a molecular-level RISM-SCF-SEDD study on the ESIPT in 1-butyl-3-methylimidazolium hexafluorophosphate ([bmim][PF_6]), which is one of the most widely used RTILs. Two new aspects are introduced. First, because the molecular geometry of solvent in the conventional RISM must be fixed at a specific one, it has not been possible to treat the conformational flexibility of [bmim][PF_6]. Here the structural fluctuation, such as the rotation of side chains, was incorporated with the aid of flexible-RISM theory.[56] The other is the nonequilibrium free-energy change due to the solvent fluctuation[60−65] along the ESIPT process. While RISM is basically a theory for equilibrium statistical mechanics, orientational polarization of solvent molecules plays an important role.[17,18] We focused on the changes in free energy and microscopic solvation to grasp the solvent relaxation of RTILs along ESIPT. To the best of our knowledge, this is the first ab initio study on photochemical reactions in RTILs.

COMPUTATIONAL DETAILS

The Kovalenko−Hirata (KH) type closure was used to solve the RISM equation.[46] The number density (ρ) of [bmim][PF_6] was set to 0.002894 molecules Å^{-3}, and the temperature T was 298.15 K, which corresponds to the experimental conditions.[1,19−21] The potential parameters of solvent [bmim][PF_6] molecules and Lennard-Jones parameters of solute molecule were taken from the literature[39,66−68] and given in Tables 1 and 2. For [bmim][PF_6] molecules, we employed the united-atom model, in which hydrogen atoms and fluoride atoms are, respectively, fused to carbon atoms and phosphorus atoms, as shown in Figure 1. The rotations of three dihedral angles along the butyl chain were taken into account using flexible-RISM theory.[56] (See the Appendix for the detailed procedure.)

Table 1. Potential Parameters for Solute and Solvent Molecules

species	site	σ/Å	ε/kcal mol^{-1}	q/|e|
DMAHF[a]	C	3.400	0.086	
	N	3.341	0.170	
	O	3.066	0.210	
	H	2.600	0.015	
	H_O[b]	1.000	0.056	
[bmim][PF_6]	C_1	3.905	0.175	−0.047
	C_2	3.905	0.118	0.118
	C_3	3.905	0.118	0.118
	C_4	3.905	0.118	0.024
	N_5	3.250	0.170	0.071
	C_6	3.880	0.106	0.229
	N_7	3.250	0.170	0.133
	C_8	3.880	0.106	0.041
	C_9	3.880	0.106	0.096
	C_{10}	3.775	0.207	0.217
	PF_6	5.600	0.399	−1.000

[a]Electrostatic interactions are determined by RISM-SCF-SEDD procedure. [b]H_O denotes the hydrogen atom attached to oxygen atoms.

Table 2. Torsional Parameters for the Rotatable Dihedral Angles[a]

dihedral angle	V_0	V_1	V_2	V_3
$C_1-C_2-C_3-C_4$	0.0000	0.7040	−0.1350	1.5740
$C_2-C_3-C_4-N_5$	0.0000	1.3360	−0.1145	0.2425
$C_3-C_4-N_5-C_6$	0.0000	−0.6980	−0.2125	0.0000
$C_3-C_4-N_5-C_9$	0.0000	−0.6980	−0.2125	0.0000

[a]All units are in kcal mol^{-1}.

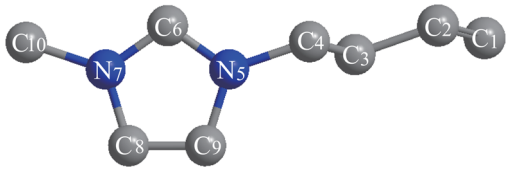

Figure 1. [bmim]$^+$ of united-atom model.

Standard 6-31G* basis sets were adopted for carbon and nitrogen atoms, and a diffuse function was added to oxygen (6-31+G*). The 6-31G basis set was used for H, while a polarization function was added to the transferring H. DFT and TDDFT with a B3LYP functional were utilized to describe the electronic structure of the solute molecule. The ethyl group in DEAHF was modeled with the methyl group, and we abbreviate the modeled molecule as DMAHF hereafter. Geometry optimizations were performed in the gas phase, and all the energy was then evaluated using the same geometries in the gas phase as well as in [bmim][PF_6].

We adopted the difference between the O_N-H and O_T-H distances as the proton coordinate q (Scheme 1)

$$q = r(O_N - H) - r(O_T - H) \quad (1)$$

For each state, the solute geometry along the proton-transfer path was determined by optimizing the other degrees of freedom at each q value. In the optimization, no symmetry constraint was applied.

All calculations for electronic structures were performed by the GAMESS suite of programs[57] modified by us to implement the RISM-SCF-SEDD method, and flexible-RISM computations were performed by our program.

RESULTS AND DISCUSSION

Free-Energy Changes. The energy profiles of S_0 and S_1 states in the gas phase and in [bmim][PF_6] along the proton coordinate q are shown in Figure 2. In the S_1 state two minima are found, which is consistent with the experimental observation of dual emission spectra. The DMAHF molecule in the S_0 state is more stable in the normal form compared with the tautomer one. The difference between the solid and dotted lines in Figure 2 corresponds to the solvation effects in energy. The molecule in the excited normal form is stabilized due to considerable solvation effects in [bmim][PF_6]. As discussed below in detail, this can be understood from the changes in the dipole moment.

The absorption and emission energies are summarized in Table 3. Here we assumed that the electronic transition to the final state is fast enough to leave the solute geometry and the solvation structure frozen at the initial state of the transition. We

dx.doi.org/10.1021/jp311883f | J. Phys. Chem. B XXXX, XXX, XXX−XXX

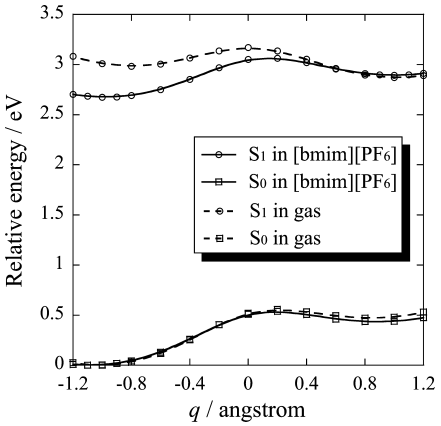

Figure 2. Relative energy as a function of the proton coordinate q with respect to the normal form in the ground state. Solid and dotted lines indicate the free energy in [bmim][PF_6] and potential energy in the gas phase, respectively. Lines with squares and circles correspond to the S_0 ground and S_1 excited state.

Table 3. Absorption and Emission Energies in Electronvolts

	calcd	exptl[20]
absorption	2.99	3.02
emission (normal)	2.34	2.34
emission (tautomer)	2.37	2.14

further assumed that the solvation is equilibrated in the excited state within the observation time-scale of the steady-state spectroscopy.[20] The latter assumption might be invalid in the case of highly viscous RTILs, whose time scale of solvation dynamics is quite slower compared with that of conventional liquids (1−10 ps). It is noted, however, that the observed fluorescent lifetime (ca. 3 ns)[20] is slightly longer compared with the time scale of [bmim][PF_6] (ca. 1 ns).[11,13] We adopted the steady-state spectrum in the present study because the fluorescence lifetime is long enough. In fact, the obtained results are in good agreement with the experimental ones, while the emission energy from the tautomer form is slightly overestimated. The works by Znamenskiy, Kobrak, or Welton et al. have shown that the spectral response can be influenced by hydrogen−bonding in [bmim][PF_6], particularly due to the C_6 site (see Figure 1).[58,59] The united-atom treatment of [bmim][PF_6] may underestimate the specific interaction and give rise to the overestimation of the emission from the excited tautomer.

Changes in Dipole Moment. Solvation effects in the free-energy profiles can be rationalized in terms of the dipole moment of solute molecules shown in Figure 3. The dipole moment becomes larger due to the excitation in the normal form, which increases the solute−solvent electrostatic interaction. The dipole moment in the excited state, however, drastically decreases as the proton transfer reaction proceeds, and thus the dipole moment of the tautomer form in the excited state is comparable to that of the ground state. These results correspond to the CIS calculations performed by Chou and collaborators,[23] although the magnitudes of their dipole moments are smaller than those of ours. The distinct solvation effects on the excited state in the normal form are consistent with the remarkable increase in the dipole moment. It is also noteworthy that a more remarkable change is induced in the S_1 state compared with that in the S_0 ground state.

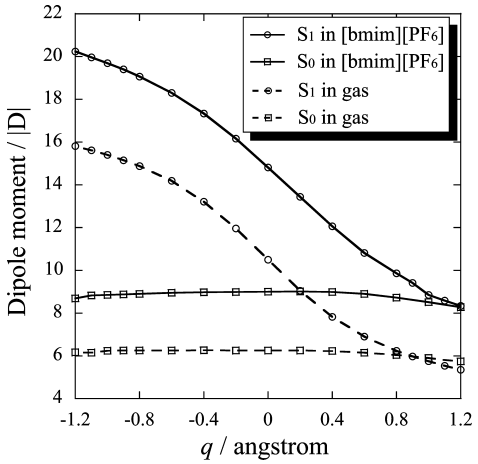

Figure 3. Changes in dipole moment along the proton coordinate q. Solid and dotted lines indicate the dipole moment in [bmim][PF_6] and in the gas phase, respectively. Lines with squares and circles correspond to the S_0 ground and S_1 excited state.

The changes in the dipole moment are consistent with the time-resolved fluorescent spectra.[19,20] While a drastic Stokes shift was observed at the normal form, no marked shift was found at the tautomer. From the changes in the dipole moment, it turns out that the electron distribution is changed due to the excitation in the normal form and the subsequent proton-transfer reaction in the excited state. The changes in the dipole moment due to the excitation can be understood from the viewpoint of molecular orbitals. TDDFT calculations revealed that the excitation can be mainly described as a HOMO(π)−LUMO(π^*) transition. Figure 4 displays important Kohn−Sham orbitals. This figure

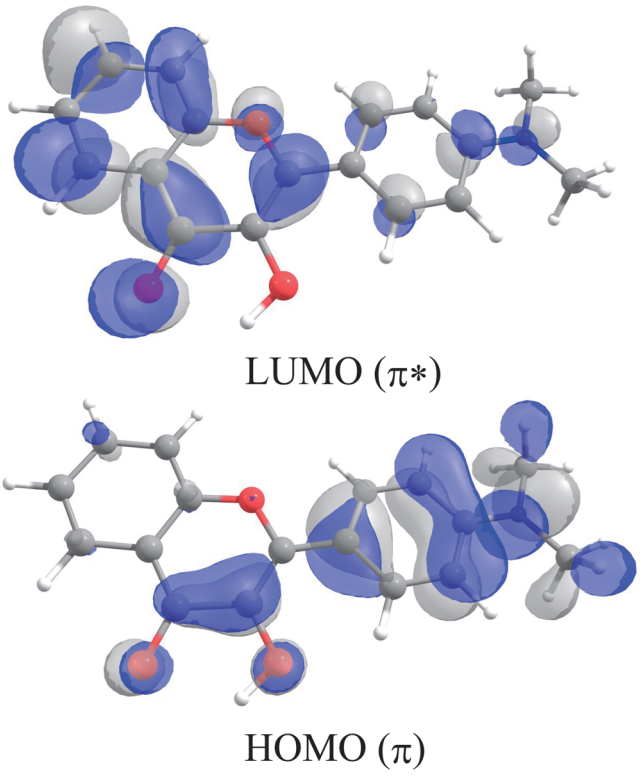

Figure 4. Important Kohn−Sham orbitals of the normal form DMAHF in [bmim][PF_6].

dx.doi.org/10.1021/jp311883f | J. Phys. Chem. B XXXX, XXX, XXX−XXX

indicates that the excitation is characterized by the electron transfer from the HOMO localized at the aniline moiety (right-hand side of DMAHF as shown in Figure 4) to the LUMO at chromene moiety (left-hand side), giving rise to the drastic increase in the dipole moment upon the excitation.

Effects of Relaxation of Solvation. *Nonequilibrium Free-Energy Change Due to Solvent Fluctuation.* The nonequilibrium free energy is given as the sum of the equilibrium free energy and the deviation from it

$$\mathcal{A}_{\mathrm{neq}}(\mathbf{R}, \mathbf{V}) = \mathcal{A}_{\mathrm{eq}}(\mathbf{R}_0, \mathbf{V}_0) + \Delta\mathcal{A}(\mathbf{R}, \mathbf{V}) \tag{2}$$

where $\mathbf{R}$ and $\mathbf{V}$ denote the solute geometry and the electrostatic potential (ESP) acting on the solute molecule, respectively. The subscript 0 stands for the equilibrium state.

The equilibrium free energy defined in the framework of RISM-SCF theory is

$$\mathcal{A}_{\mathrm{eq}}(\mathbf{R}_0, \mathbf{V}_0) = \left\langle \Psi_{\mathrm{sol}}(\mathbf{R}_0, \mathbf{V}_0) | \hat{H}(\mathbf{R}_0) | \Psi_{\mathrm{sol}}(\mathbf{R}_0, \mathbf{V}_0) \right\rangle + \Delta\mu_0(\mathbf{R}_0, \mathbf{V}_0) \tag{3}$$

Here, $\hat{H}$ is the Hamiltonian for a solute molecule in the standard quantum chemical method and Ψ_{sol} is the wave function of the solute molecule in solution. In the framework of RISM with KH closure, the solvation free energy $\Delta\mu_0$ is analytically given as[46]

$$\Delta\mu_0(\mathbf{R}_0, \mathbf{V}_0) = \sum_{\alpha}^{\text{solute}} \sum_{\gamma}^{\text{solvent}} \frac{4\pi\rho_\gamma}{\beta} \int \mathrm{d}r\, r^2 \left\{ \frac{1}{2}(h_{\alpha\gamma}(r))^2 \Theta(h_{\alpha\gamma}(r)) - c_{\alpha\gamma}(r) - \frac{1}{2} h_{\alpha\gamma}(r) c_{\alpha\gamma}(r) \right\} \tag{4}$$

where $h_{\alpha\gamma}(r)$ and $c_{\alpha\gamma}(r)$ are the total and direct correlation functions, respectively. β is the inverse of the product of the Boltzmann constant k_{B} and temperature T. Θ is the Heaviside step function. ρ_γ denotes the density of the solvent site γ.

Here we assumed that the deviation from the equilibrium free energy can be considered as the change due to the solvent fluctuation. Chong et al. have proposed a method to evaluate the nonequilibrium free-energy profile in the electron-transfer process, which was further extended to quantum mechanical systems.[60−65] We modify the method to evaluate $\Delta\mathcal{A}$ so as to adapt the RISM-SCF-SEDD method, in which the charge distribution of the solute molecule is expressed with the expansion coefficient of auxiliary basis sets (ABSs) $\mathbf{d}$.[44,45] To calculate the distribution functions for nonequilibrium processes, we introduce a hypothetical charge distribution and solute geometry, as a function of the linear parameter s, for describing solvent fluctuation due to the excitation

$$\mathbf{d}^s = (1 - s)\mathbf{d}_{S_0} + s\mathbf{d}_{S_1} \tag{5}$$

and

$$\mathbf{R}^s = (1 - s)\mathbf{R}_{S_0} + s\mathbf{R}_{S_1} \tag{6}$$

To express the solvent fluctuation due to the proton transfer, we adopted a coordinate q, which denotes the equilibrium state parameter at a specific proton coordinate

$$\mathbf{d}^q = \mathbf{d}(q) \tag{7}$$

and

$$\mathbf{R}^q = \mathbf{R}(q) \tag{8}$$

Combining s and q, we generated the solvent configurations corresponding to the fluctuation due to the excitation and the proton-transfer reaction in the excited state.

In the model (a schematic illustration is shown in Figure 5), "nonequilibrium" solvent configuration $\mathbf{V}^{s,q}(\mathbf{d}^{s,q})$ can be realized as an "equilibrium" state by setting $\mathbf{d}^{s,q}$ corresponding to the hypothetical charge on solute molecules. With the same procedure described in the previous papers,[62−64] the expression of the nonequilibrium free energy change is given by

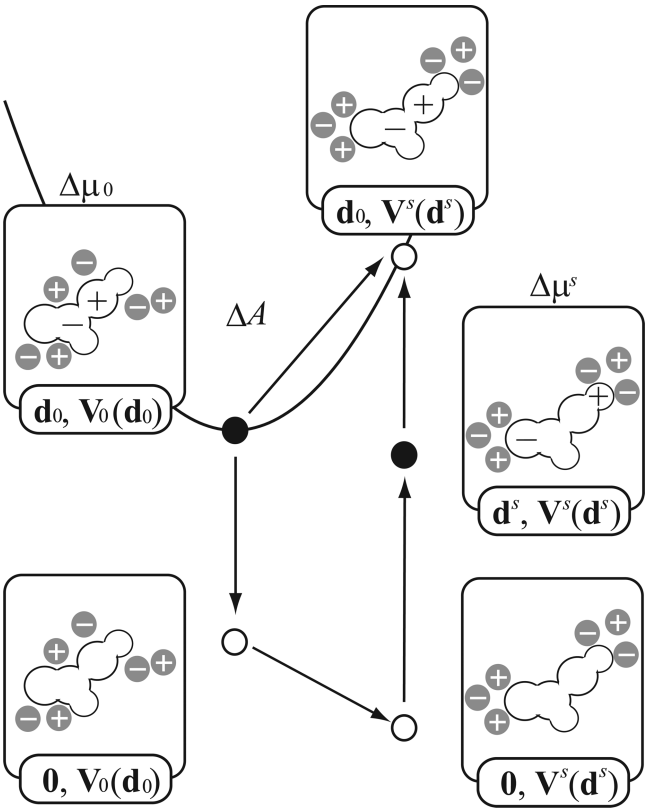

Figure 5. Schematic illustration for the nonequilibrium free energy due to solvent fluctuation in the framework of RISM-SCF-SEDD based on the thermodynamic cycle model.[62−64] The solvent configuration is schematically represented by gray circles with positive or negative signs. The charge distributions and solvent configurations are denoted by the two variables $\mathbf{d}$ and $\mathbf{V}(\mathbf{d})$. Black circles represent the equilibrium states obtained by standard RISM calculations.

$$\Delta\mathcal{A}(\mathbf{R}^{s,q}, \mathbf{V}^{s,q}) = \Delta\mu^{s,q} - \Delta\mu_0 - \mathbf{V}^{s,q}(\mathbf{d}^{s,q} - \mathbf{d}_0) \tag{9}$$

where the solvent ESP $V^{s,q}$ acting on ABSs can be expressed in the framework of RISM-SCF-SEDD[44,45] as follows:

$$\mathbf{V}^{s,q} = \sum_{i}^{\text{ABSs}} V_i^{s,q} = \sum_{i}^{\text{ABSs}} \sum_{\gamma}^{\text{solvent}} \rho_\gamma q_\gamma C_i \left(\frac{\pi}{\alpha_i}\right)^{3/2} \int_0^\infty \mathrm{d}r\, 4\pi r^2 \frac{\mathrm{erf}(\sqrt{\alpha_i} r) h_{\alpha\gamma}^{s,q}(r)}{r} \tag{10}$$

dx.doi.org/10.1021/jp311883f | J. Phys. Chem. B XXXX, XXX, XXX−XXX

C_i and α_i stand for the coefficients and exponents of ABSs. $\Delta\mu^{s,q}$ can be obtained by substituting the correlation functions calculated with the hypothetical $\mathbf{d}^{s,q}$ and geometry into eq 4. From eqs 2, 3, and 9, the final form for the nonequilibrium free energy is given by

$$\mathcal{A}_{neq}(\mathbf{R}^{s,q}, \mathbf{V}^{s,q}) = \left\langle \Psi_{sol}(\mathbf{R}_0, \mathbf{V}_0)|\hat{H}(\mathbf{R}_0)|\Psi_{sol}(\mathbf{R}_0, \mathbf{V}_0)\right\rangle + \Delta\mu^{s,q}(\mathbf{R}^{s,q}, \mathbf{V}^{s,q}) - \mathbf{V}^{s,q}(\mathbf{d}^{s,q} - \mathbf{d}_0) \quad (11)$$

Evolution of Proton Transfer Potential. We chose the difference between the electrostatic interaction energies following a standard method as the solvation coordinate corresponding to the solvent fluctuation in the ESIPT process

$$\Delta H^{s,q} = \mathbf{V}^{s,q}(\mathbf{d}_{S_1}^{normal} - \mathbf{d}_{S_1}^{tautomer}) \quad (12)$$

Figure 6 shows the free-energy surface of the S_1 state.[69] The energy plotted there is that calculated relative to the equilibrium

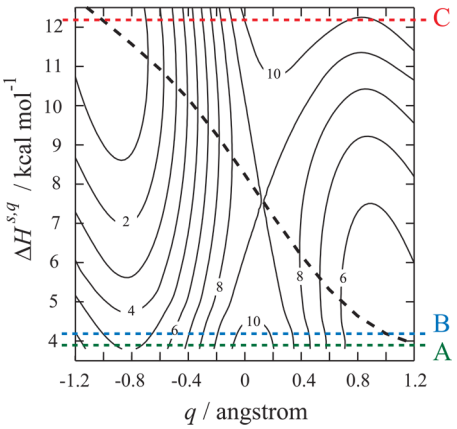

Figure 6. Nonequilibrium free energy calculated relative to that of the equilibrium excited-state normal form ($\Delta\mathcal{A}_{neq}$). Contour spacings are 1.0 kcal mol^{-1}. The dotted thick line stands for the equilibrium free-energy solvation path, which corresponds to the free-energy curve of the S_1 state in Figure 2. The green, blue, and red lines correspond to the solvation coordinate (A) immediately after the excitation, (B) the equilibrium excited-state tautomer form, and (C) the normal form, respectively.

free energy of the excited state in the normal form. Note that the free-energy changes with respect to the solvent fluctuation (vertical direction) can be well-approximated with quadratic functions (see Supporting Information for the Stokes shift in the normal form), although the method employed here is inherently a nonlinear theory. The linear response regime provides a good approximation for this system, similarly to the preceding papers.[70−76] The potential energy change of the proton transfer under the fixed field of the solvent molecules gives us insight into the evolution of the proton transfer process coupled to the solvent orientational polarization.[54,77,78] In particular, we focused on the solvent configurations immediately after the excitation (corresponding to $\Delta H^{s,q} \simeq 3.9$ kcal mol^{-1} and $q < 0$: we call the region "A") and equilibrium solvation after the relaxation, which are consistent with the excited tautomer form ($\Delta H^{s,q} \simeq 4.2$ kcal mol^{-1} and $q > 0$: region "B") and the excited normal form ($\Delta H^{s,q} \simeq 12.2$ kcal mol^{-1} and $q < 0$: region "C"). Figure 7 shows the energy change of the transfer in the excited state, corresponding to the cross sections at fixed $\Delta H^{s,q}$. In the region A (green), the barrier height of the proton transfer is relatively

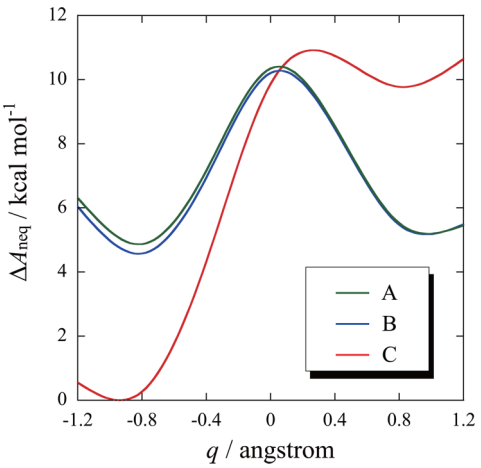

Figure 7. Nonequilibrium free energy changes $\Delta\mathcal{A}_{neq}$ along the proton coordinate q. See the text and Figure 6 for the definitions of curves A−C.

small because the solvent configuration is unfavorable for the normal form. Through the relaxation toward the equilibrium, the solvation configuration becomes consistent with the normal form (red: region C). Eventually, the excited normal form is strongly stabilized, while the excited tautomer is apparently unstable. This suggests that the barrier becomes higher as the solvent relaxes toward the normal form, corresponding to the dynamic Stokes shift observed in the experiments.[19−21] The energy profile, in which the solvation configuration is consistent with the tautomer form (blue: region B), is rather similar to that in the region A. This can be understood in terms of the dipole moment (Figure 3) and the solvation coordinate (Figure 7). The dipole moment and $\Delta H^{s,q}$ in the tautomer are similar to those of the region C.

It should be noted that adiabatic proton transfer, in which the proton quantum subsystem responds promptly to the solvent configuration,[18,79] is assumed here. The importance of tunneling effects on proton-transfer process in many systems has been pointed out.[79,80] In this case, however, because the proton transfer process is triggered by light, the effects would be less serious compared with the typical case, in which the transfer is induced by thermal fluctuation.

Although a quantitative description of time-dependent phenomena is not available from the free-energy surface, the relation between solvent relaxation and the ESIPT process is understood with the aid of experimental observations.[19−24] Experimentally, faster (∼3 ps) and slower (20−30 ps) ESIPT processes were observed not only in RTILs but also in acetonitrile,[20] which suggests that a reaction with two distinct time constants does not arise from the inherent properties of RTILs. The solvation dynamics of RTILs is much slower than the ESIPT process on a nanosecond time scale. On the basis of these observations, it seems that the proton transfer mostly proceeds under the solvation coordinate with small $\Delta H^{s,q}$ (corresponding to the green line in Figure 6). After the completion of the ESIPT in the initial stage, the solvent relaxation to the excited-state normal form proceeds along the solvation coordinate. The solvation coordinate near the region A may be dominated by local translations of the ions in the vicinity of the solute, as previously suggested.[14−16]

We further paid attention to the dependency of the proton-transfer rate upon the excitation wavelength. When DEAHF in RTILs is excited with long (short)-wavelength light, the ratio of

dx.doi.org/10.1021/jp311883f | J. Phys. Chem. B XXXX, XXX, XXX−XXX

the normal (tautomer) is increased.[20,21] This can be interpreted based on the free-energy contour. When the excitation wavelength is high (low), the initial value of $\Delta H^{s,q}$ is large (small), and thus the barrier height of the proton potential is high (low), giving rise to an increase in the ratio of the normal (tautomer). It is noted, however, that the energy difference between the surfaces of the S_1 and S_0 states should be strictly considered. The excitation wavelength dependence cannot be perfectly understood only with the free-energy contour, because it is closely related to time-dependent properties, such as the slow relaxation of environmental solvent.[81]

Solvent Configurations. Typically, solvation structures are investigated using radial distribution functions $g(r)$. [bmim]-[PF_6] is, however, composed of many sites, and it is difficult to identify solvation structure by ascribing specific configurations of solvent. Thus we focused on charge-density functions that reduce solvent configurations to distributions of solvent charge

$$\rho_\alpha(r) = \sum_{\gamma}^{\text{solvent site}} \rho_\gamma q_\gamma g_{\alpha\gamma}(r) \tag{13}$$

Figure 8 represents changes in the charge density around O_T along the relaxation (a) from immediately after the excitation to the normal form in the excited state mainly attributed to the change in $\Delta H^{s,q}$ and (b) from immediately after the excitation to the tautomer related to the change in q. In regions where the functions are positive, the contribution from the $[bmim]^+$ is dominant, while in regions where the functions are negative, the main contribution comes from $[PF_6]^-$. In the charge density functions in Figure 8a, a sharp positive peak is found at 3.3 Å, indicating that the main contribution in the first solvation shell is from the cations, which directly contact O_T. A small negative peak is found at 4.7 Å, indicating that the anions do not contact with O_T directly. The contribution is attributed to the transferring H. As the relaxation to the normal form proceeds, the positive peak is enhanced, while the negative peak diminishes. This is because O_T is more negatively charged due to the charge transfer from the amine moiety. In the charge density functions in Figure 8b, a sharp peak is found at 3.3 Å as well, where the peak height is lowered as the solvation structure relaxes to the tautomer. The peak position and height of a small negative peak found at 5 Å become closer and higher along the relaxation. These changes arise from the formation of a bond between O_T and H.

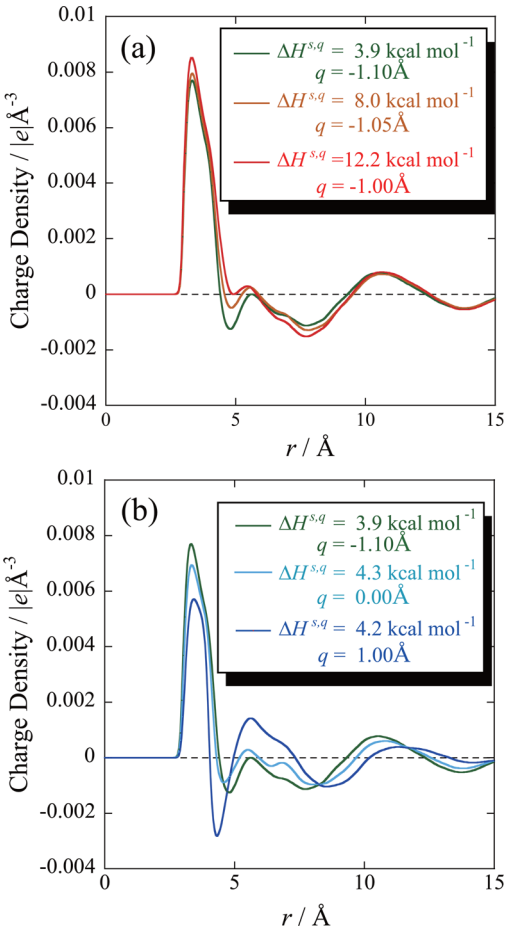

Figure 8. Changes in charge density functions around O_T along the relaxation (a) from immediately after the excitation to the excited-state normal form and (b) from immediately after the excitation to the excited-state tautomer. The orange and cyan curves represent states intermediate to the excited normal and tautomer states; see the inset and Figure 6 for details.

CONCLUSIONS

We theoretically investigated the ESIPT of the DMAHF molecule in [bmim][PF_6] using the RISM-SCF-SEDD method in conjunction with flexible-RISM. To incorporate the non-equilibrium solvation effects due to solvent fluctuation concomitant with the photo-excitation and proton-transfer process, we utilized a thermodynamic treatment proposed by Chong et al.

The free-energy curves along the proton coordinate q exhibit two important features: the normal form is more stable in the ground state and two minima are found in the excited state, which is consistent with the experimental observations. The calculated absorption and emission energy are in good agreement with the experiments. The excitation is mainly characterized by the electron transfer from the HOMO on aniline moiety to the LUMO on chromene moiety, giving rise to the drastic increase in the dipole moment of DMAHF. This corresponds to the observed dynamic Stokes shift of the peak assigned to the excited normal form. The proton transfer in the excited state is also accompanied by drastic changes in the dipole moment. The nonequilibrium free-energy contour as a function of the proton coordinate q and the solvation coordinate $\Delta H^{s,q}$ gives us two insights into this system: (i) the evolution of proton potential and (ii) the validity of the linear response approximation. While immediately after the excitation the barrier height of the proton transfer process is relatively small, the barrier becomes larger as the solvation relaxation to the excited normal state proceeds. The experimental observations and the obtained results suggest that the ESIPT process is completed in the solvation coordinate near the region A, namely, in the initial stage of the photo-excitation. The result obtained here and in the preceding papers suggests that the linear response free energy, in which the distribution of solvent fluctuations is represented by a Gaussian form,[52,54,82−84] is applicable to various ionic liquid systems.

Before closing, we draw the readers' attention to the dependency of the rate of proton transfer on the excitation wavelength.[20,21] Very recently, the excitation wavelength dependence was explored in relation to the inhomogeneous distribution of the solute in RTILs.[21] It is reported that the spacial inhomogeneous structure[76,85−91] is not crucial for the

dx.doi.org/10.1021/jp311883f | J. Phys. Chem. B XXXX, XXX, XXX−XXX

excitation wavelength dependence because a similar effect is observed for conventional molecular liquids. The excitation wavelength dependence is observed through energetic heterogeneity, while the relation between the spatial inhomogeneous structure in RTILs and the energetic heterogeneity has not been perfectly clarified yet. Further theoretical studies with some improved treatments on the relation between the reaction dynamics of the ESIPT of DEAHF and inhomogeneous solvation are highly desired.

APPENDIX: INCORPORATING STRUCTURAL FLUCTUATION OF [BMIM]$^+$

The solvent−solvent RISM equation, which gives correlation functions for neat liquids, is written as follows[92]

$$\mathbf{h}_{vv} = \boldsymbol{\omega}_v{}^*\mathbf{c}_{vv}{}^*\boldsymbol{\omega}_v + \boldsymbol{\omega}_v{}^*\mathbf{c}_{vv}{}^*\boldsymbol{\rho}_v\mathbf{h}_{vv} \tag{14}$$

Here $\boldsymbol{h}$ and $\boldsymbol{c}$ are the matrices of total and direct correlation functions, respectively. $\boldsymbol{\rho}$ is that of the number density of solvent, and $\boldsymbol{\omega}$ denotes the matrix of intramolecular correlation functions, which is represented by delta functions for rigid molecules. The subscript v indicates solvent. In flexible-RISM theory, the intramolecular structural fluctuation of solvent molecules is treated in terms of intramolecular correlation functions $\boldsymbol{\omega}$, which are decomposed into an ideal gas part, $\boldsymbol{\omega}^{\mathrm{ref}}$, and a residual part, $\Delta\boldsymbol{\omega}$, as

$$\boldsymbol{\omega} = \boldsymbol{\omega}^{\mathrm{ref}} + \Delta\boldsymbol{\omega} \tag{15}$$

$\boldsymbol{\omega}^{\mathrm{ref}}$ is evaluated with Monte Carlo simulations for an isolated molecule, and $\Delta\boldsymbol{\omega}$, which describes many-body effects in liquids, is iteratively determined by solving the developed equations.[56]

In the RISM computations of the ionic liquid, only four dihedral angles were flexible in this model, namely, $C_1-C_2-C_3-C_4$, $C_2-C_3-C_4-N_5$, $C_3-C_4-N_5-C_6$, and $C_3-C_4-N_5-C_9$. The bond lengths and bond angles were fixed at the geometry of $\boldsymbol{\omega}^{\mathrm{ref}}$ determined by optimizing isolated [bmim]$^+$ at the MP2/6-311G(d,p) level. The potential for these dihedral angles $V(\phi)$ is expressed as

$$V(\phi) = V_0 + \sum_{n=1}^{3} V_n[1 - (-1)^n \cos(n\phi)] \tag{16}$$

where the parameters employed for four dihedral angles in [bmim]$^+$ are summarized in Table 2.[66,67] The standard Monte Carlo simulation for $\boldsymbol{\omega}^{\mathrm{ref}}$ of isolated [bmim]$^+$ using the Metropolis algorithm was carried out with 300 million configuration generations.

Solvation effects on solute molecules are incorporated through the solute−solvent RISM equation[92]

$$\mathbf{h}_{uv} = \boldsymbol{\omega}_u{}^*\mathbf{c}_{uv}{}^*\boldsymbol{\chi}_{vv} \tag{17}$$

$$\mathbf{h}_{uv} = \boldsymbol{\omega}_u{}^*\mathbf{c}_{uv}{}^*\boldsymbol{\omega}_v + \boldsymbol{\omega}_u{}^*\mathbf{c}_{uv}{}^*\boldsymbol{\rho}_v\mathbf{h}_{vv} \tag{18}$$

The subscript u stands for solute. We can solve the equation by obtaining the solvent susceptibility, $\boldsymbol{\chi}_{vv}$, with flexible-RISM theory to incorporate solvation effects in flexible solvent molecules.

ASSOCIATED CONTENT

Supporting Information

Nonequilibrium free-energy changes corresponding to the Stokes shift in the excited-state normal form. This material is available free of charge via the Internet at http://pubs.acs.org.

AUTHOR INFORMATION

Corresponding Author

*E-mail: hirofumi@moleng.kyoto-u.ac.jp.

Notes

The authors declare no competing financial interest.

ACKNOWLEDGMENTS

We are grateful to Ms. Kayo Suda, Dr. Daisuke Yokogawa, and Dr. Kentaro Kido for invaluable discussions, providing the flexible-RISM program, and providing the multicomponent RISM program, respectively. The work is financially partially supported by Grant-in-Aid for Scientific Research on Priority Areas 'Molecular Science for Supra Functional Systems' (477-22018016), Grant-in-Aid for Scientific Research on Innovative Areas 'Molecular Science of Fluctuations' (2006-21107511), Grant-in-Aid for Scientific Research (B) (23350006), as well as by Grant-in-Aid for Scientific Research (C) (20550013). S.H. acknowledges the Grant-in Aid for JSPS Fellows. The Strategic Programs for Innovative Research (SPIRE), the Computational Materials Science Initiative (CMSI), and the Ministry of Education, Culture, Sports, Science and Technology (MEXT) of Japan are also acknowledged.

REFERENCES

(1) *Ionic Liquids in Synthesis*, 2nd ed.; Welton, T., Wasserscheid, P., Eds.; VCH-Wiley: Weinheim, Germany, 2008.
(2) Weingärtner, H. Understanding Ionic Liquids at the Molecular Level: Facts, Problems, and Controversies. *Angew. Chem., Int. Ed.* **2008**, *47*, 654−670.
(3) Castner, E. D.; Wishart, J. F. Spotlight on Ionic Liquids. *J. Chem. Phys.* **2010**, *132*, 120901.
(4) Castner, E. W., Jr.; Margulis, C. J.; Maroncelli, M.; Wishart, J. F. Ionic Liquids: Structure and Photochemical Reactions. *Annu. Rev. Phys. Chem.* **2011**, *62*, 85−105.
(5) Karmakar, R.; Samanta, A. Solvation Dynamics of Coumarin-153 in a Room-Temperature Ionic Liquids. *J. Phys. Chem. A* **2002**, *106*, 4447−4452.
(6) Karmakar, R.; Samanta, A. Dynamics of Solvation of the Fluocescent State of Some Electron-Donor Acceptor Molecules in Room Temperature Ionic Liquids, [BMIM][$(CF_3SO_2)_2$N] and [EMIM][$(CF_3SO_2)_2$N]. *J. Phys. Chem. A* **2003**, *107*, 7340−7346.
(7) Paul, A.; Samanta, A. Solute Rotation and Solvation Dynamics in an Alcohol-Functionalized Room Temperature Ionic Liquids. *J. Phys. Chem. B* **2007**, *111*, 4724−4731.
(8) Ingram, J. A.; Moog, R. S.; Ito, N.; Biswas, R.; Maroncelli, M. Solute Rotation and Solvation Dynamics in a Room-Temperature Ionic Liquid. *J. Phys. Chem. B* **2003**, *107*, 5926−5932.
(9) Arzhantsev, S.; Ito, N.; Heitz, M.; Maroncelli, M. Solvation Dynamics of Coumarin 153 in Several Classes of Ionic Liquids: Cation Dependence of the Ultrafast Component. *Chem. Phys. Lett.* **2003**, *381*, 278−286.
(10) Arzhantsev, S.; Jin, H.; Baker, G. A.; Maroncelli, M. Measurement of the Complete Solvation Response in Ionic Liquids. *J. Phys. Chem. B* **2007**, *111*, 4978−4989.
(11) Jin, H.; Baker, G. A.; Arzhantsev, S.; Dong, J.; Maroncelli, M. Survey of Solvation and Rotational Dynamics of Coumarin 153 in a Broad Range of Ionic Liquids and Comparisons to Conventional Solvents. *J. Phys. Chem. B* **2007**, *111*, 7291−7302.
(12) Seth, D.; Chakraborty, A.; Setua, P.; Sarkar, N. Dynamics of Solvent and Rotational Relaxation of Coumarin-153 in Room-Temperature Ionic Liquid 1-Butyl-3-methyl Imidazolium Tetrafluoroborate Confined in Poly(oxyethylene glycol) Ethers Containing Micelles. *J. Phys. Chem. B* **2007**, *111*, 4781−4787.
(13) Nagasawa, Y.; Itoh, T.; Yasuda, M.; Ishibashi, Y.; Ito, S.; Miyasaka, H. Ultrafast Charge Transfer Process of 9,9′-Bianthryl in Imidazolium Ionic Liquids. *J. Phys. Chem. B* **2008**, *112*, 15758−15765.

(14) Shim, Y.; Duan, J. S.; Choi, M. Y.; Kim, H. J. Solvation in Molecular Ionic Liquids. *J. Chem. Phys.* **2003**, *119*, 6411−6414.
(15) Shim, Y.; Choi, M. Y.; Kim, H. J. A Molecular Dynamics Computer Simulation Study of Room-Temperature Ionic Liquids. II. Equilibrium and Nonequilibrium Solvation Dynamics. *J. Chem. Phys.* **2005**, *122*, 044511.
(16) Kobrak, M. N. Characterization of the Solvation Dynamics of a Room-Temperature Ionic Liquid via Molecular Dynamics Simulation. *J. Chem. Phys.* **2006**, *125*, 064502.
(17) *Chemical Dynamics in Condensed Phase*, 1st ed.; Nitzan, A., Ed.; Oxford University Press: New York, 2006.
(18) *Charge and Energy Transfer Dynamics in Molecular Systems*, 3rd ed.; May, V., Kühn, O., Eds.; VCH-Wiley: Weinheim, Germany, 2011.
(19) Fukuda, M.; Terazima, M.; Kimura, Y. Study on the Excited State Intramolecular Proton Transfer of 4′-*N*,*N*-Diethylamino-3-hydroxyflavone in Imidazolium-Based Room Temperature Ionic liquids. *Chem. Phys. Lett.* **2008**, *463*, 364−368.
(20) Kimura, Y.; Fukuda, M.; Suda, K.; Terazima, M. Excited State Intramolecular Proton Transfer Reaction of 4′-*N*,*N*-Diethylamino-3-hydroxyflavone and Solvation Dynamics in Room Temperature Ionic Liquids Studied by Optical Kerr Gate Fluorescence Measurement. *J. Phys. Chem. B* **2010**, *114*, 11847−11858.
(21) Suda, K.; Terazima, M.; Kimura, Y. Excitation Wavelength Dependence of Photo-Induced Intramolecular Proton Transfer Reaction of 4′-*N*,*N*-Diethylamino-3-hydroxyflavone in Various Liquids. *Chem. Phys. Lett.* **2012**, *531*, 70−74.
(22) Chou, P. T.; Huang, C. H.; Pu, S. C.; Cheng, Y. M.; Yu, W. S.; Yu, Y. C.; Wang, Y.; Chen, C. T. The Dipolar Functionality Tuning Excited-State Charge/Proton Transfer Coupled Reaction. *J. Phys. Chem. A* **2004**, *108*, 6452−6454.
(23) Chou, P. T.; Pu, S. C.; Cheng, Y. M.; Yu, W. S.; Yu, Y. C.; Hung, F. T.; Hu, W. P. Femtosecond Dynamics on the Excited-State Proton/Charge Transfer Coupled Reaction in 4′-*N*,*N*-Diethylamino-3-hydroxyflavones. *J. Phys. Chem. A* **2005**, *109*, 3777−3787.
(24) Cheng, Y. M.; Pu, S. C.; Yu, Y. C.; Chou, P. T.; Huang, C. H.; Chen, C. T.; Li, T. H.; Hu, W. P. Spectroscopy and Femtosecond Dynamics of 7-*N*,*N*-Diethylamino-3-hydroxyflavone; Generalization of Dipolar Tuning Excited-State Proton/Charge Transfer Reaction. *J. Phys. Chem. A* **2005**, *109*, 11696−11706.
(25) Mandal, P. K.; Sarkar, M.; Samanta, A. Excitation-Wavelength-Dependent Fluorescence Behaviour of Some Dipolar Molecules in Room-Temperature Ionic Liquids. *J. Phys. Chem. A* **2004**, *108*, 9048−9053.
(26) Paul, A.; Mandal, P. K.; Samanta, A. On the Optical Properties of the Imidazolium Ionic Liquids. *J. Phys. Chem. B* **2005**, *109*, 9148−9153.
(27) Jin, H.; Xiang, Li.; Maroncelli, M. Heterogeneous Solute Dynamics in Room-Temperature Ionic Liquids. *J. Phys. Chem. B* **2007**, *111*, 13473−13478.
(28) Kimura, Y.; Hamamoto, T.; Terazima, M. Raman Spectroscopic Study on the Solvation of *N*,*N*-Dimethyl-*p*-nitroaniline in Room-Temperature Ionic Liquids. *J. Phys. Chem. A* **2007**, *111*, 7081−7089.
(29) Acevedo, O.; Jorgensen, W. L.; Evanseck, J. D. Elucidation of Rate Variations for a Diels-Alder Reaction in Ionic Liquids from QM/MM Simulations. *J. Chem. Theor. Comput.* **2007**, *3*, 132−138.
(30) Sambasivarao, S. V.; Acevedo, O. Development of OPLS-AA Force Field Parameters for 68 Unique Ionic Liquids. *J. Chem. Theory Comput.* **2009**, *5*, 1038−1050.
(31) Arantes, G. M.; Ribeiro, M. C. C. A Microscopic View of Substitution Reactions Solvated by Ionic Liquids. *J. Chem. Phys.* **2008**, *128*, 114503.
(32) Yockel, S.; Schatz, G. C. Modeling $O(^3P)$ and Ar Scattering from the Ionic Liquid [emim][NO_3] at 5 eV with Hybrid QM/MM Molecular Dynamics. *J. Phys. Chem. B* **2010**, *114*, 14241−14248.
(33) Li, X.; Schatz, G. C.; Nesbitt, D. J. Anion Effects in the Scattering of CO_2 from the Room-Temperature Ionic Liquids [bmim][BF_4] and [bmim][Tf_2N]: Insights from Quantum Mechanics/Molecular Mechanics Trajectories. *J. Phys. Chem. B* **2012**, *116*, 3587−3602.
(34) Klähn, M.; Seduraman, A.; Wu, P. Proton Transfer between Tryptophan and Ionic Liquid Solvents Studied with Molecular Dynamics Simulations. *J. Phys. Chem. B* **2011**, *115*, 8231−8241.
(35) Chandler, D.; Anderson, H. C. Optimized Cluster Expansions for Classical Fluids. II. Theory of Molecular Liquids. *J. Chem. Phys.* **1972**, *57*, 1930−1937.
(36) Hirata, F.; Rossky, P. J. An Extended RISM Equation for Molecular Polar Fluids. *Chem. Phys. Lett.* **1981**, *83*, 329−334.
(37) Kinoshita, M.; Hirata, F. Analysis of Salt Effects on Solubility of Noble Gases in Water Using the Reference Interaction Site Model Theory. *J. Chem. Phys.* **1997**, *106*, 5202−5215.
(38) Bruzzone, S.; Malvaldi, M.; Chiappe, C. A RISM Approach to the Liquid Structure and Solvation Properties of Ionic Liquids. *Phys. Chem. Chem. Phys.* **2007**, *9*, 5576−5581.
(39) Bruzzone, S.; Malvaldi, M.; Chiappe, C. Solvation Thermodynamics of Alkali and Halide Ions in Ionic Liquids through Integral Equations. *J. Chem. Phys.* **2008**, *129*, 074509.
(40) Yamaguchi, T.; Koda, S. Mode-Coupling Theoretical Analysis of Transport and Relaxation Properties of Liquid Dimethylimidazolium Chloride. *J. Chem. Phys.* **2010**, *132*, 114502.
(41) Ten-no, S.; Hirata, F.; Kato, S. A Hybrid Approach for the Solvent Effect on the Electronic Structure of a Solute Based on the RISM and Hartree-Fock Equations. *Chem. Phys. Lett.* **1993**, *214*, 391−396.
(42) Ten-no, S.; Hirata, F.; Kato, S. Reference Interaction Site Model Self-Consistent Field Study for Solvation Effect on Carbonyl Compounds in Aqueous Solution. *J. Chem. Phys.* **1994**, *100*, 7443−7453.
(43) Sato, H.; Hirata, F.; Kato, S. Analytical Energy Gradient for the Reference Interaction Site Model Multiconfigurational Self-Consistent-Field Method: Application to 1,2-Difluoroethylene in Aqueous Solution. *J. Chem. Phys.* **1996**, *105*, 1546−1551.
(44) Yokogawa, D.; Sato, H.; Sakaki, S. New Generation of the Reference Interaction Site Model Self-Consistent Field Method: Introduction of Spatial Electron Density Distribution to the Solvation Theory. *J. Chem. Phys.* **2007**, *126*, 244054.
(45) Yokogawa, D.; Sato, H.; Sakaki, S. Analytical Energy Gradient for Reference Interaction Site Model Selfconsistent Field Explicitly Including Spatial Electron Density Distribution. *J. Chem. Phys.* **2009**, *131*, 214504.
(46) Kovalenko, A.; Hirata, F. Self-Consistent Description of a Metal−water Interface by the Kohn-Sham Density Functional Theory and the Three-Dimensional Reference Interaction Site Model. *J. Chem. Phys.* **1999**, *110*, 10095−10112.
(47) Malvaldi, M.; Bruzzone, S.; Chiappe, C.; Gusarov, S.; Kovalenko, A. *Ab Initio* Study of Ionic Liquids by KS-DFT/3D-RISM-KH Theory. *J. Phys. Chem. B* **2009**, *113*, 3536−3542.
(48) Chiappe, C.; Malvaldi, M.; Pomelli, C. S. *Ab Initio* Study of the Diels-Alder Reaction of Cyclopentadiene with Acrolein in a Ionic Liquid by KS-DFT/3D-RISM-KH Theory. *J. Chem. Theory Comput.* **2010**, *6*, 179−183.
(49) Hayaki, S.; Kido, K.; Yokogawa, D.; Sato, H.; Sakaki, S. A Theoretical Analysis of a Diels-Alder Reaction in Ionic Liquids. *J. Phys. Chem. B* **2009**, *113*, 8227−8230.
(50) Hayaki, S.; Kido, K.; Sato, H.; Sakaki, S. *Ab initio* Study on S_N2 Reaction of Methyl p-Nitrobenzenesulfonate and Chloride Anion in [mmim][PF_6]. *Phys. Chem. Chem. Phys.* **2010**, *12*, 1822−1826.
(51) Yamazaki, S.; Kato, S. Excited-State Proton Transfer of 1-[(Dimethylamino)methyl]-2-naphthol in Acetonitrile solvent: RISM-SCF and MRMP Approach. *Chem. Phys. Lett.* **2004**, *386*, 414−418.
(52) Yamamoto, T.; Kato, S. *Ab initio* Calculation of Proton-Coupled Electron Transfer Rates Using the External-Potential Representation: A Ubiquinol Complex in Solution. *J. Chem. Phys.* **2007**, *126*, 224514.
(53) Aono, S.; Kato, S. Proton Transfer in Phenol−Amine Complexes: Phenol Electronic Effects on Free Energy Profile in Solution. *J. Comput. Chem.* **2010**, *31*, 2924−2931.
(54) Aono, S.; Yamamoto, T.; Kato, S. Proton Transfer in Phenol/Amine Complexes: Phenol Electronic Effects on Free Energy Profile in Solution. *J. Chem. Phys.* **2011**, *134*, 144108.
(55) Inagaki, T.; Yamamoto, T.; Kato, S. Proton-Coupled Electron Transfer of the Phenoxyl/Phenol Couple: Effect of Hartree-Fock

Exchange on Transition Structures. *J. Comput. Chem.* **2011**, *32*, 3081−3091.
(56) Yokogawa, D.; Sato, H.; Sakaki, S. An Integral Equation Theory for Structural Fluctuation in Molecular Liquid. *Chem. Phys. Lett.* **2010**, *487*, 241−245.
(57) Schmidt, M. W.; Baldridge, K. K.; Boatz, J. A.; Elbert, S. T.; Gordon, M. S.; Jensen, J. H.; Koseki, S.; Matsunaga, N.; Nguyen, K. A.; Su, S.; Windus, T. L.; et al. General Atomic and Molecular Electronic Structure System. *J. Comput. Chem.* **1993**, *14*, 1347−1363.
(58) Znamenskiy, V.; Kobrak, M. N. Molecular Dynamics Study of Polarity in Room-Temperature Ionic Liquids. *J. Phys. Chem. B* **2004**, *108*, 1072−1079.
(59) Crowhurst, L.; Mawdsley, P. R.; Perez-Arlandis, J. M.; Salter, P. A.; Welton, T. Solvent-Solute Interactions in Ionic Liquids. *Phys. Chem. Chem. Phys.* **2003**, *5*, 2790−2794.
(60) Chong, S.-H.; Miura, S.; Basu, G.; Hirata, F. Molecular Theory for the Nonequilibrium Free Energy Profile in Electron Transfer Reaction. *J. Phys. Chem.* **1995**, *99*, 10526−10529.
(61) Chong, S.-H.; Hirata, F. Nonlinear Electrical Potential Fluctuations of Solvent around Solutes: An Integral Equation Study. *J. Chem. Phys.* **1997**, *106*, 5225−5238.
(62) Sato, H.; Hirata, F. Equilibrium and Nonequilibrium Solvation Structure of Hexaammineruthenium (II, III) in Aqueous Solution: *Ab Initio* RISM-SCF Study. *J. Phys. Chem. A* **2002**, *106*, 2300−2304.
(63) Sato, H.; Kobori, Y.; Tero-Kubota, S.; Hirata, F. Theoretical Study of Electronic and Solvent Reorganization Associated with a Charging Process of Organic Compounds. I. Molecular and Atomic Level Description of Solvent Reorganization. *J. Chem. Phys.* **2003**, *119*, 2753−2760.
(64) Sato, H.; Kobori, Y.; Tero-Kubota, S.; Hirata, F. Theoretical Study on Electronic and Solvent Reorganization Associated with a Charging Process of Organic Compounds. 2. A New Decomposition Procedure into Electrostatic and Nonelectrostatic Responses. *J. Phys. Chem. B* **2004**, *108*, 11709−11715.
(65) Yoshida, N.; Ishida, T.; Hirata, F. Theoretical Study of Temperature and Solvent Dependence of the Free-Energy Surface of the Intramolecular Electron-Transfer Based on the RISM-SCF Theory: Application to the 1,3-Dinitrobenzene Radical Anion in Acetonitrile and Methanol. *J. Phys. Chem. B* **2008**, *112*, 433−440.
(66) Shah, J. K.; Brennecke, J. F.; Maginn, E. J. Thermodynamic Properties of the Ionic Liquid 1-*n*-Butyl-3-methylimidazolium Hexafluorophosphate from Monte Carlo Simulations. *Green Chem.* **2002**, *4*, 112−118.
(67) Shah, J. K.; Maginn, E. J. Monte Carlo Simulations of Gas Solubility in the Ionic Liquid 1-*n*-Butyl-3-methylimidazolium Hexafluorophosphate. *J. Phys. Chem. B* **2005**, *109*, 10395−10405.
(68) Cornell, W. D.; Cieplak, P.; Bayly, C. I.; Gould, I. R.; Merz, K. M., Jr.; Fergunson, D. M.; Spellmeyer, D. C.; Fox, T.; Caldwell, J. W.; Kollman, P. A. A Second Generation Force Field for the Simulation of Proteins, Nucleic Acids, and Organic Molecules. *J. Am. Chem. Soc.* **1995**, *117*, 5179−5197.
(69) Because the ESPs are generated from specific geometries along the restrictive proton coordinate q (−1.2 Å < q < 1.2 Å), the resultant energy of region nearby $\Delta H^{s,q} \simeq 3.8$ kcal mol^{-1} and q = −1.2 Å is not obtained. This is because the minimum of $\Delta H^{s,q}$ along the vertical axis at q = −1.2 Å is the farthest from the region $\Delta H^{s,q} \simeq 3.8$ kcal mol^{-1}. The region is not essential for the following discussion, and thus cubic spline extrapolation was performed to obtain the contour.
(70) Lynden-Bell, R. M. Does Marcus Theory Apply to Redox Processes in Ionic Liquids? A Simulation Study. *Electrochem. Commun.* **2007**, *9*, 1857−1861.
(71) Lynden-Bell, R. M. Can Marcus Theory Be Applied to Redox Processes in Ionic Liquids? A Comparative Simulation Study of Dimethylimidazolium Liquids and Acetonitrile. *J. Phys. Chem. B* **2007**, *111*, 10800−10806.
(72) Lynden-Bell, R. M. Redox Potentials and Screening in Ionic Liquids: Effects of Sizes and Shapes of Solute Ions. *J. Chem. Phys.* **2008**, *129*, 204503.
(73) Streeter, I.; Lynden-Bell, R. M.; Compton, R. G. Nonlinear Relaxation in Redox Processes in Ionic and Polar Liquids. *J. Phys. Chem. C* **2008**, *112*, 14538−14544.
(74) Shim, Y.; Kim, H. J. Free Energy and Dynamics of Electron Transfer Reactions in a Room-Temperature Ionic Liquid. *J. Phys. Chem. B* **2007**, *111*, 4510−4519.
(75) Shim, Y.; Jeong, D.; Manjari, S.; Choi, M. Y.; Kim, H. J. Solvation, Solute Rotation and Vibration Relaxation, and Electron Transfer Reactions in Room-Temperature Ionic Liquids. *Acc. Chem. Res.* **2007**, *40*, 1130−1137.
(76) Annapureddy, H. V. R.; Margulis, J. Controlling the Outcome of Electron Transfer Reactions in Ionic Liquids. *J. Phys. Chem. B* **2009**, *113*, 12005−12012.
(77) Ando, K.; Hynes, J. T. Molecular Mechanism of HCl Acid Ionization in Water: *Ab Initio* Potential Energy Surfaces and Monte Carlo Simulations. *J. Phys. Chem. B* **1997**, *101*, 10464−10478.
(78) Ando, K.; Hynes, J. T. Molecular Mechanism of HF Acid Ionization in Water: An Electronic Structure-Monte Carlo Study. *J. Phys. Chem. A* **1999**, *103*, 10398−10408.
(79) Hammes-Schiffer, S.; Stuchebrukhov, A. A. Theory of Coupled Electron and Proton Transfer Reactions. *Chem. Rev.* **2010**, *110*, 6939−6960.
(80) Pu, J.; Gao, J.; Truhlar, D. G. Multidimensional Tunneling, Recrossing, and the Transmission Coefficient for Enzymatic Reactions. *Chem. Rev.* **2006**, *106*, 3140−3169.
(81) Demchenko, A. P. The Red-Dege Effects: 30 Years of Exploration. *Luminescence.* **2002**, *17*, 19−42.
(82) Yamazaki, S.; Kato, S. Locating the Lowest Free-Energy Point on Conical Intersection in Polar Solvent: Reference Interaction Site Model Self-Consistent Field Study of Ethylene and $CH_2NH_2^+$. *J. Chem. Phys.* **2005**, *123*, 114510.
(83) Higashi, M.; Kato, S. Theoretical Study on Electronic and Spin Structures of $[Fe_2S_2]^{2+,+}$ Cluster: Reference Interaction Site Model Self-Consistent Field (RISM-SCF) and Multireference Second-Order Mø ller-Plesset Perturbation Theory (MRMP) Approach. *J. Phys. Chem. A* **2005**, *109*, 9867−9874.
(84) Mori, T.; Nakano, K.; Kato, S. Conical Intersections of Free Energy Surfaces in Solution: Effect of Electron Correlation on a Protonated Schiff Base in Methanol Solution. *J. Chem. Phys.* **2010**, *133*, 064107.
(85) Wang, Y.; Voth, G. A. Unique Spatial Heterogeneity in Ionic Liquids. *J. Am. Chem. Soc.* **2005**, *127*, 12192−12193.
(86) Wang, Y.; Voth, G. A. Multiscale Coarse-Graining of Ionic Liquids. *J. Phys. Chem. B* **2006**, *110*, 18601−18608.
(87) Canongia Lopes, J. N. A.; Pádua, A. A. H. Nanostructural Organization in Ionic Liquids. *J. Phys. Chem. B* **2006**, *110*, 3330−3335.
(88) Shigeto, S.; Hamaguchi, H. A New Nonlinear Raman Probe for Local Structures in Liquids and Solutions. *Chem. Phys. Lett.* **2006**, *417*, 329−332.
(89) Iwata, K.; Okajima, H.; Saha, S.; Hamaguchi, H. Local Structure Formation in Alkyl-imidazolium-Based Ionic Liquids as Revealed by Linear and Nonlinear Raman Spectroscopy. *Acc. Chem. Res.* **2007**, *40*, 1174−1181.
(90) Triolo, A.; Russina, O.; Bleif, H.-J.; Cola, E. D. Nanoscale Segregation in Room Temperature Ionic Liquids. *J. Phys. Chem. B* **2007**, *111*, 4641−4644.
(91) Hu, Z.; Margulis, C. J. Heterogeneity in a Room-Temperature Ionic Liquid: Persistent Local Environments and the Red-Edge Effect. *Proc. Natl. Acad. Sci. U. S. A.* **2006**, *103*, 831−836.
(92) For example , *Molecular Theory of Solvation*; Hirata, F., Ed.; Kluwer Academic Publishers: Dordrecht, The Netherlands, 2003.